A two-sublattice model for extracting rare-earth anisotropy constants from measurements on (Nd,Ce)2(Fe,Co)14B single crystals

Gabriel Gomez Eslava, Bahar Fayyazi, Konstantin Skokov, Yurii Skourski, Denis Gorbunov, Oliver Gutfleisch, Nora M Dempsey, Dominique Givord

A two-sublattice model for extracting rare-earth anisotropy constants from measurements on $(Nd,Ce)_2(Fe,Co)_{14}B$ single crystals

Gabriel Gomez Eslava[1], Bahar Fayyazi[2], Konstantin Skokov[2], Yurii Skourski[3], Denis Gorbunov[3], Oliver Gutfleisch[2], Nora M. Dempsey[1] and Dominique Givord[1†]

[1]Univ. Grenoble Alpes, Grenoble INP, Institut Néel, 38000 Grenoble, France
[2]Technical University Darmstadt, Institute of Material Science, 64287 Darmstadt, Germany
[3] Dresden High Magnetic Field Laboratory (HLD-EMFL), Helmholtz-Zentrum Dresden-Rossendorf, D-01328 Dresden, Germany

Abstract

Anisotropy constants are obtained from an analysis of single crystal magnetization curves measured up to high fields. The anisotropy of the 3*d* transition metal (M) sublattice is considered, as well as molecular exchange field coupling between the rare-earth (R) and transition metal sublattices (M). This procedure allows for non colinear R and M magnetic moments, meaning that their angles with respect to the easy axis are independent variables. With this approach we obtain anisotropy constants that are larger than those reported in the literature, which reflects the anisotropy of the isolated R sublattice. Results for Co and/or Ce doped $Nd_2Fe_{14}B$ single crystals are presented, showing the influence of such substitutions on the magnetocrystalline anisotropy. These results indicate that the enhanced performance of NdFeB-based magnets co-doped with Ce and Co is due to an improvement in intrinsic properties.

1. Introduction

High-performance permanent magnets are critical components for modern energy technologies such as wind turbines and electro-mobility. Permanent magnets based on the $Nd_2Fe_{14}B$ compound set the benchmark, due to their excellent magnetic properties at room temperature. However, for high-temperature applications, their coercivity has been enhanced by the addition of Dy and Tb, which are considered as highly critical elements [1, 2]. The world's most sought-after rare-earth elements are Nd, Pr, Dy, Tb, Y, and Eu, which are used in the production of magnets and luminescent materials. Owing to the chemical similarity of the R elements, the above-mentioned rare earths are found and mined together with other rare-earth elements such as Ce and La. There is much less demand for the latter elements and therefore an excess of them is currently available. This situation is known as the *rare earth balance problem* [3]. Ce is the most abundant rare-earth element and is the cheapest of all rare earths. Therefore, the development of (Ce-Nd)-based permanent magnets would be both cost efficient and a strategic way to utilize R resources.

---

† D.O.D. 4th February 2019

$Ce_2Fe_{14}B$ crystalizes in the same crystal structure as $Nd_2Fe_{14}B$. However, as a result of different valance states of the R elements, their magnetism is distinct. Whereas Nd is trivalent in $Nd_2Fe_{14}B$, Ce fluctuates between 3+ and 4+ in $Ce_2Fe_{14}B$ [4], At room temperature, the saturation magnetization (M_s) of $Ce_2Fe_{14}B$ is 23.9 μ_B/f.u, which is 26% lower than that of $Nd_2Fe_{14}B$; the anisotropy field (H_a) of $Ce_2Fe_{14}B$ is 2.6 T, which is 3 times lower than that of $Nd_2Fe_{14}B$ ($\mu_0 H_a$ =8T); the Curie temperature of $Ce_2Fe_{14}B$ is 424 K whereas that of $Nd_2Fe_{14}B$ is 585 K [5]. Accordingly, the substitution of Ce in NdFeB magnets leads to a deterioration of the intrinsic magnetic properties. Nevertheless, by optimizing the composition and applying microstructure engineering, decent magnetic properties have been obtained in Ce containing NdFeB permanent magnets [5-9]. The effect of additional elemental substitutions to compensate losses resulting from Ce substitution have been reported in the literature. The partial substitution of Co for Fe in (Nd,Ce)-Fe-B increases the Curie temperature, due to enhanced exchange interactions. On the other hand, references [10,11] report that in a limited substitutional range, Co preferentially occupies the 4*c* and 8j_1 M sites, which show a stronger affinity with the R elements than the other M sites. DFT calculations of Co-doped $Ce_2Fe_{14}B$ predict that, by altering the coordination conditions, the valance state of Ce shifts towards 3+ [12], and in a sweet spot concentration range of Ce and Co, improved magnetic properties can be obtained [13]. An enhancement of magnetic properties of Ce and Co co-doped Nd-Fe-B magnets, especially at room temperature and above (relevant for permanent magnet applications) are reported in [8,13-15]. Whether the enhanced properties are related to microstructural effects or are intrinsic in origin i.e., enhanced magnetocrystalline anisotropy, has not yet been established.

This study is dedicated to a precise determination of the magnetocrystalline anisotropy of Ce and/or Co substituted $Nd_2Fe_{14}B$ compounds. While the most reliable magnetic data can be obtained from measurements on high quality single crystals, firstly, the synthesis and measurement procedures are not straightforward and secondly, they are very time consuming. Therefore, in recent years, modelling methods have been developed for the calculation of intrinsic magnetic properties [16,17]. Here we combine experimental measurements on single crystals of $Nd_2Fe_{14}B$, $(Nd_{0.85}Ce_{0.15})_2Fe_{14}B$, $Nd_2(Fe_{0.9}Co_{0.1})_{14}B$ and $(Nd_{0.9}Ce_{0.1})_2(Fe_{0.85}Co_{0.15})_{14}B$ with modelling based on crystalline-electric field (CEF) calculations and the molecular field approximation, to extract anisotropy constants. To do this, we consider a two sublattice model, i.e., we consider separate contributions from the rare-earth (R) and from the transition metal (M) sub-lattices. This method differs from the vast majority of results presented in literature, as it provides anisotropy constants specific to the R sub-lattice, instead of mean values for the whole material, as is the case with the single lattice model. The validation of the two-sublattice model opens opportunities for predicting the magnetic properties on a wider concentration range and in even more complicated systems, to guide the optimization of magnet development.

2. Experimental details

Taking advantage of the coexistence of the desirable 2:14:1 phase and liquid R phase in the phase diagram of NdFeB, single crystals were grown using the “reactive flux” method [18]. Off-stoichiometric $(Nd_{1-x}Ce_x)_{33.5}(Fe_{1-y}Co_y)_{62.5}B_4$ alloys with (1) x=0 and y=0, (2) x=0.2 and y=0, (3) x=0 and y=0.15 and (4) x=0.2 and y=0.15 were prepared by induction melting of high purity elements in zirconia crucibles under argon atmosphere. The precursors were sealed in an evacuated quartz ampule, homogenized at 1070°C for 2 days and subsequently slowly cooled

down at a rate of 0.5K/h. Nd-(Fe,Co)-B samples were cooled to 690°C while Ce containing samples were cooled to 930°C to avoid the formation of $CeFe_2$, which becomes stable below this temperature. The samples were annealed for 100 hours at the final temperature and subsequently quenched in water. From the obtained microstructure, many needle-shaped single crystals were extracted (Figure 1.a). The chemical composition of the resulting 2:14:1 single crystals was determined using Energy Dispersive X-ray (EDX) spectroscopy equipped in a Philips XL30 FEG Scanning Electron Microscopy (SEM). The single crystallinity and crystallographic orientation of the single crystals were verified using a back-scattering Laue camera. The isothermal magnetization up to 14 T was measured using a Physical properties Measurement System (PPMS 14, Quantum Design) with vibrating Sample Magnetometer (VSM) option along [100] and [110] crystallographic orientations at temperatures ranging from 10 to 300 K. For magnetization measurements at fields up to 60 T, a pulsed-field magnetometer built at the High-field Laboratory in Dresden-Rossendorf (HZDR), described in detail in [19], was used.

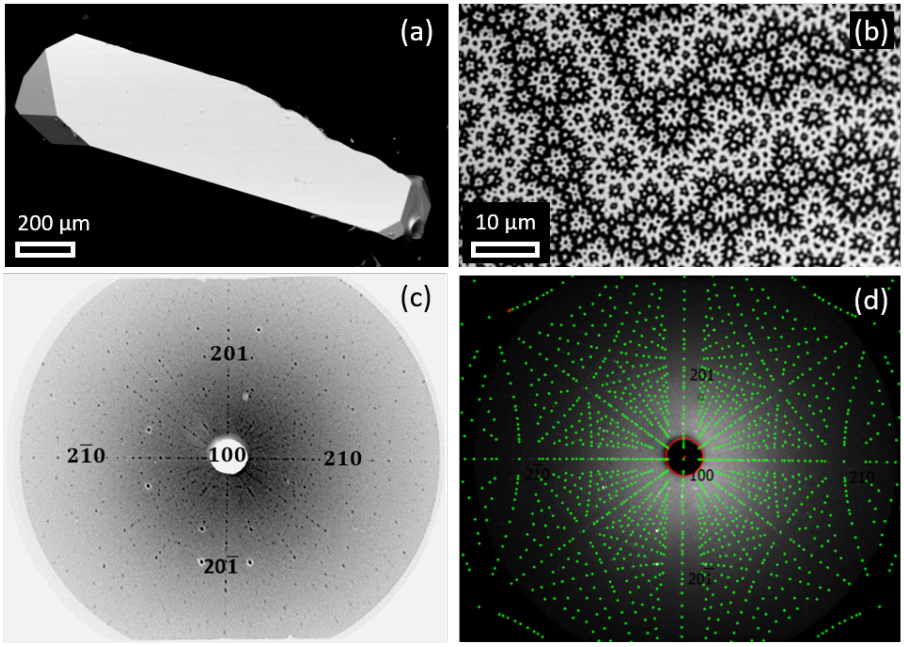

Figure 1. (a) SEM image of a $(Nd_{0.85}Ce_{0.15})_2(Fe_{0.9}Co_{0.1})_{14}B$ single crystal used for magnetic measurements. (b) The uniaxial domain structure of the 2:14:1 phase observed by MOKE microscope along the c-axis. (c) Laue X-ray diffraction pattern with incident beam along [100] of the crystal. (d) Simulated pattern of the corresponding structure given by Clip software.

3. Two sublattice model

The usual way to describe the magnetic properties of R-M intermetallics is to calculate magnetization curves based on a minimization of the energy of the system. When considering the expression for the total energy, different approaches can be found in the literature. The most common one is to consider that the M and R moments are always colinear for a given applied field and temperature [20]. This approach, known as the single-lattice model (SL), does not discriminate between the contributions to the total anisotropy and magnetization coming from the M and R sub-lattices individually. The physics behind the inter-sublattice coupling is thus somehow hidden. Furthermore, non-collinearity between M and R magnetic moments has been experimentally evidenced. As an example, a spin reorientation transition

(SRT) occurring at low temperatures when R=Nd, Ho, Er, Tm and Yb, arises from the misalignment of M and R sublattices, with the degree of misalignment growing as the temperature decreases. In the late 80's Cadogan et al. [21] proposed a new method in order to deduce the anisotropy constants and crystal field parameters of $Nd_2Fe_{14}B$, taking into consideration the 3d-4f exchange coupling in the total free energy expression. Based on this method, the authors deduced a non-colinear magnetic structure at 4.2 K. In the same year Yamada et al. [22] presented a more comprehensive discussion about the effects of crystal and molecular field on the magnetic properties of $R_2Fe_{14}B$ compounds. In addition to the exchange interaction between R and Fe sublattices, the authors consider also the first excited multiplet (J=11/2) of the Nd atoms, in order to calculate the anisotropy energy at finite temperature. The authors showed that this effect is rather small in Nd and Pr compounds. Explicit values of the anisotropy constants K_i were not reported. It is important to remark that the relationship between crystal field parameters and K_i at finite temperature is still not fully understood. Additional evidence comes from polarized neutron scattering and Mossbauer experiments, the results of which are satisfactorily explained by the noncollinearity of R and M moments at temperatures below the SRT, as pointed out by Herbst et al. [23].

More recently Miura et al. [24] discussed the importance of considering the R-M inter sublattice exchange in order to correctly evaluate the temperature evolution of the magnetic anisotropy. The authors present a comparison between colinear and non-colinear magnetic moments, focusing on the effect of non-collinearity in compounds with heavy rare-earths, as its analysis is simpler due to the absence of a spin reorientation transition. A strategy for calculating the anisotropy constants is discussed, assuming a small deviation (perturbative approach) when non-collinearity effects are considered.

Here we present a semi-classical two-sublattice model (TL), which is similar to that proposed by Cadogan et al. [21] and Yamada et al. [22]. In order to calculate the magnetization of the R sublattice at 0 K (M_R) we use a similar form of the Hamiltonian proposed by those authors. Thus, the energy spectrum of the R atom at 0 K is obtained by taking into account the Fe-R exchange (molecular field) and explicitly including the first anisotropy constant of the Fe sublattice. The latter is introduced as a phenomenological value, assumed to be the same as in $Y_2Fe_{14}B$ [25]. Quantum effects are only considered for the calculation of energy level splitting of the R atom at 0 K. At finite temperatures the thermal population of the different energy levels is set assuming a Boltzmann distribution. No J-mixing effects at finite temperatures are considered. As has been demonstrated by Yamada et al. the contribution of excited states at finite temperature are negligible for Nd compounds.

We consider that, when a magnetic field is applied along the hard direction at a given temperature, the individual M and R magnetic moments are free to rotate independently, within the plane containing the magnetic field vector. The total energy of the system under the applied field is given by the expression:

$$E = E_A + E_{Exch} + E_Z \quad (1)$$

Where E_A is the anisotropy energy, E_{Exch} is the exchange energy between the two sublattices due to the molecular field and E_Z is the Zeeman energy. The anisotropy energy of a tetragonal structure, due to the CEF, is described in terms of the direction cosines:

$$E_A = K_M \sin^2 \vartheta_M + K_1 \sin^2 \vartheta_R + (K_2 + K_2' \cos 4\varphi) \sin^4 \vartheta_R + (K_3 + K_3' \cos 4\varphi) \sin^6 \vartheta_R \quad (2)$$

Where K_M is the second order anisotropy constant of the transition metal, as obtained experimentally for $Y_2Fe_{14}B$ [25]. K_1, K_2 and K_3 are the second, fourth and sixth order anisotropy constants of the rare earth, respectively. K_2' and K_3' are the fourth and sixth order anisotropy constants associated with basal plane anisotropy. ϑ_M and ϑ_R are the angles between the easy axis of magnetization (c-axis) and the M and R magnetic moments, respectively. Finally, φ is the angle formed by the [100] direction and the basal plane projection of the magnetization.

The exchange energy can be written as:

$$E_{Exch} = -n_{RM} \langle M_M \rangle_T \langle M_R \rangle_T \cos(\vartheta_M - \vartheta_R) \quad (3)$$

Where $\langle M_M \rangle_T$ is the magnetization of the M sublattice at temperature T, deduced from the $M_s(T)$ curve of $Y_2Fe_{14}B$, using the Kuz'min formula [26,27] with s=0.6 and the Curie temperature, T_c, calculated following the procedure described in [17]. $\langle M_R \rangle_T$ is the thermal average of the R magnetization at temperature T, calculated from the total angular moment of the R atom at zero temperature [16]. The exchange constant n_{RM} represents the molecular field interaction, with the molecular field acting on the R spin moment [28].

Assuming that the in-plane projection of $\mathbf{M}_s$ is always aligned with the in-plane direction of the magnetic field, the Zeeman energy, E_Z, is given by the usual expression:

$$E_z = \boldsymbol{B}_{app} \cdot \boldsymbol{M}_s = -B_{app} [\langle M_M \rangle_T \sin \vartheta_M + \langle M_R \rangle_T \sin \vartheta_R] \quad (4)$$

All the energy terms above can be extended to a second R atom, as described in [17].

In order to reproduce the experimental conditions, we need to set φ to a proper value. For the magnetic field applied along the [100] direction $\varphi = 0$, so that the anisotropy energy (eq. (2)) becomes:

$$E_A = K_M \sin^2 \vartheta_M + K_1 \sin^2 \vartheta_R + K_2^+ \sin^4 \vartheta_R + K_3^+ \sin^6 \vartheta_R \quad (5)$$

Where $K_i^+ = K_i + K_i'$; $i = 2,3$. In a similar way, for the field applied along the [110] direction ($\varphi = \pi/4$), the anisotropy energy becomes:

$$E_A = K_M \sin^2 \vartheta_M + K_1 \sin^2 \vartheta_R + K_2^- \sin^4 \vartheta_R + K_3^- \sin^6 \vartheta_R \quad (6)$$

Where $K_i^- = K_i - K_i'$; $i = 2,3$.

Thus, by reproducing the experimental plots we are able to determine the $K_i^{\pm}$ constants via a fitting process, so that the individual values for all the R anisotropy constants can be obtained. In order to do that, for each temperature and direction we adjust the values of three fitting parameters, namely K_1, $K_2^{\pm}$ and $K_3^{\pm}$, in order to obtain a curve that best reproduces the experimental magnetization curve. For a given field, the total energy is

numerically minimized in terms of ϑ_M and ϑ_R as independent variables. Then, the total magnetization (M_T) is calculated as the summation of the in-plane projection of M and R magnetization, for the critical value of the angles, ϑ_M^c and ϑ_R^c:

$$M_T = M_M \sin\vartheta_M^c + M_R \sin\vartheta_R^c \quad (7)$$

In the next sections we apply the method described above in order to determine the anisotropy constants of the four single crystal samples described in the experimental section.

4. $Nd_2Fe_{14}B$ single crystal

M(H) curves were analyzed by using the TL method described in the previous section. In Fig. 2 we show the results of the calculated curves at 10 and 300 K. Thermal expansion of the crystal lattice are neglected, since the thermal expansion of the compound is about 0.6% in the temperature range of interest [29]. Firstly K_1, $K_2^+$and K_3^+parameters are adjusted to fit the curve along the [100] direction. At low temperature, specifically below the spin reorientation temperature, T_{SR}, the fitted curved is calculated respecting the initial magnetization ($\mu_0 H$=0), the critical field and the critical magnetization just before the first order magnetization process (FOMP). Then, while keeping the same value of K_1, the parameters $K_2^-$and K_3^- are varied to calculate *M(H)* along the [110] direction. The same procedure is followed for the other temperatures. In Fig. 2 we show calculated (black continous lines) and measured magnetization curves along the [100] direction (blue open symbols), [110] direction (red open symbols) at 10 K and 250 K. We can see that the in-plane anisotropy is still present at 250 K. Some anisotropy is also detected at 300 K (not shown). In general, the agreement between calculated and measured curves is very good.

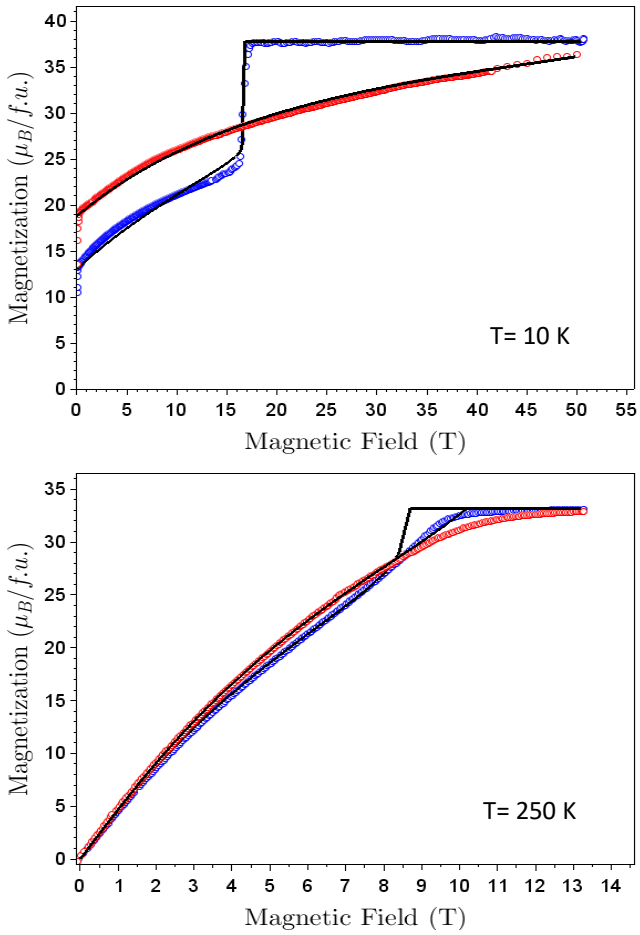

Figure 2. Open symbols: M(H) curves measured on a single crystal of $Nd_2Fe_{14}B$ at 10 K and 250 K, along the [100] (blue) and [110] (red) directions. The black lines are calculated curves (see text).

By combining the fitting parameters $K_i^+$and K_i^- obtained at a given temperature, individual values of the anisotropy constants K_2, K_2', K_3 and K_3' are obtained, as shown in Fig. 3. At about 150 K, near T_{SR}, K_1 changes sign from negative to positive. Above 150 K K_1 becomes positive and is much larger than all the other constants at RT, consistent with the uniaxial anisotropy character of the material at $T_{SR} \leq T \leq T_c$. At lower temperatures the dominant terms are the higher order constants K_2, K_2', K_3 and K_3'. Anisotropy constants from Bolzoni et al. [20] (open symbols), extracted from a SL model, are also included in Fig. 3. Similar results were reported by Cadogan et al. [21] and Yamada et al. [22]. At low temperature, the absolute values of the anisotropy constants obtained with our TL model are significantly higher than those obtained from SL models. For the sake of comparison, we also reanalysed our *M(H)*

data by using our own SL model, as shown by dashed lines in Fig. 3. To perform those calculations, we modified equations (2) and (3) by neglecting inter-lattice exchange and 3*d* anisotropy contributions to the total energy (Eq. (1)). Also, colinearity between R and M moments was imposed, i. e. $\vartheta_R = \vartheta_M = \vartheta$, which is equivalent to having n_{RM} tending to infinity. The uniaxial anisotropy constants K_1, K_2 and K_3, obtained by our SL model are in fair agreement with Bolzoni et al. [20] However, for the in-plane constants K_2' and K_3'our SL model leads to slightly higher absolute values.

Focusing on the TL model, larger values of the anisotropy constants can be expected, as the anisotropy of the M sublattice is much smaller than that of the R sublattice. This creates a tendency for the M moments to rotate towards the direction of the applied field faster than the R moments. This idea is supported by the evolution of M and R critical angles (see Fig. 4), obtained during the calculation of the magnetization curves of Fig. 2. Below the saturation field, the curves corresponding to ϑ_R^c (red) are below the curve of ϑ_M^c (blue). Thanks to exchange coupling between the two sublattices, the larger anisotropy of the R atom prevents the rotation of both R and M magnetic moments. Saturation of magnetization (total rotation) happens only when the magnetic field is intense enough to rotate R moments. It is important to note that the contribution to the total magnetization coming from the M sublattice is at least five times larger than that coming from the R sublattice. This means that very large anisotropy energy is required in the R sublattice in order to prevent rotation of the total magnetization induced by the applied field. The anisotropy constants obtained by the SL method are representative of the compound as a whole, rather than the anisotropy of the R sublattice, as in the TL model presented here. Attempts to model the temperature dependence of the anisotropy constants, based on the formalism of Stevens' operators, have led to higher values of the anisotropy constants at very low temperatures compared to values obtained experimentally [16]. This can be explained by the fact that for such calculations, the angle of the R and M magnetic moments are treated as independent variables (non-collinearity). This means that the predicted values in the literature are related solely to the R sublattice, whereas the experimental values are obtained for the material as a whole. Thus, our new approach to extract the anisotropy constants by using a TL model seems more appropriate in order to directly compare calculated and experimental values (see reference [16] for instance).

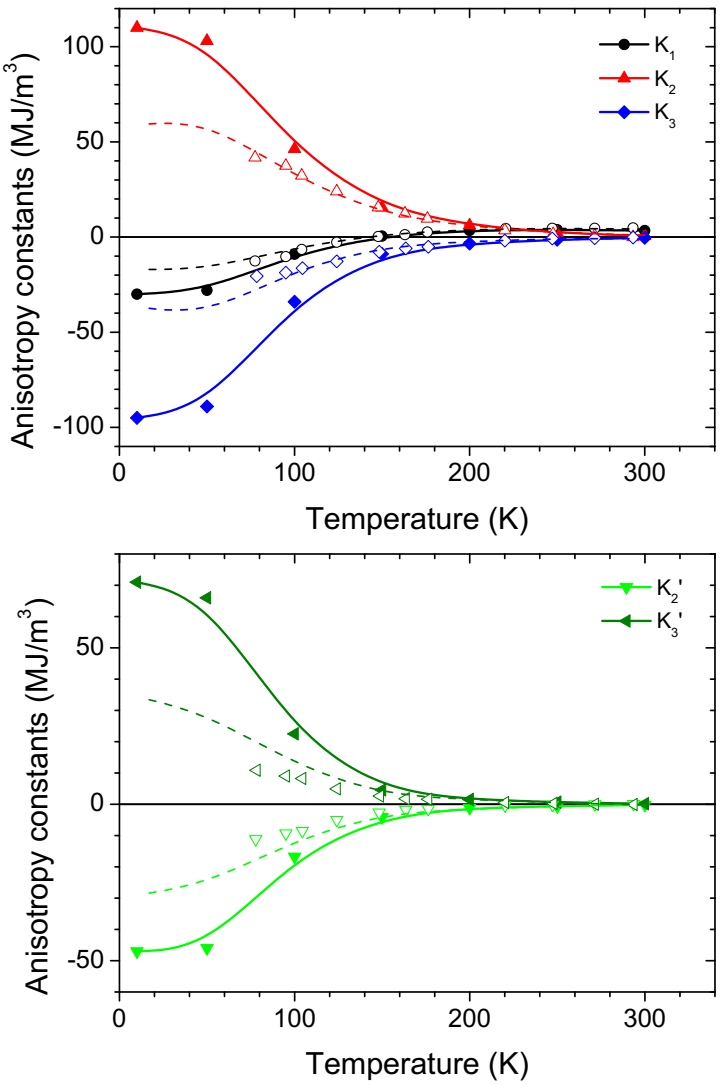

Figure 3. Anisotropy constants as a function of the temperature of a $Nd_2Fe_{14}B$ single crystal, extracted from a TL model (solid symbols) and from a SL model (dashed lines) and those reported by Bolzoni et al. [20] from a SL model (open symbols). Solid lines are a guide to the eye.

Monte Carlo calculations of the magnetic properties of $Nd_2Fe_{14}B$, considering a TL model, have been reported by Toga et al. [30] and Gong et al. [31]. Concerning anisotropy constants, both authors compare their calculated values with experimental data from K. D. Durst and H. Kronmuller [32] (only K_1 and K_2 anisotropy constants are presented). In Toga et al. and Gong et al. the calculation of the anisotropy constants is done by considering a total energy expression characteristic of a TL model. In contrast, the values reported by Durst and Kronmuller were extracted from a SL model. A very good agreement between TL calculations and SL experimental data is found in both publications, which is somewhat surprising. In our work we make a direct comparison between TL and SL lattice models, including results from Bolzoni et al. [20], which are in agreement with those of Durst and Kronmuller. A significant difference in our results obtained from the two different models was found, especially at low T (Fig. 3).

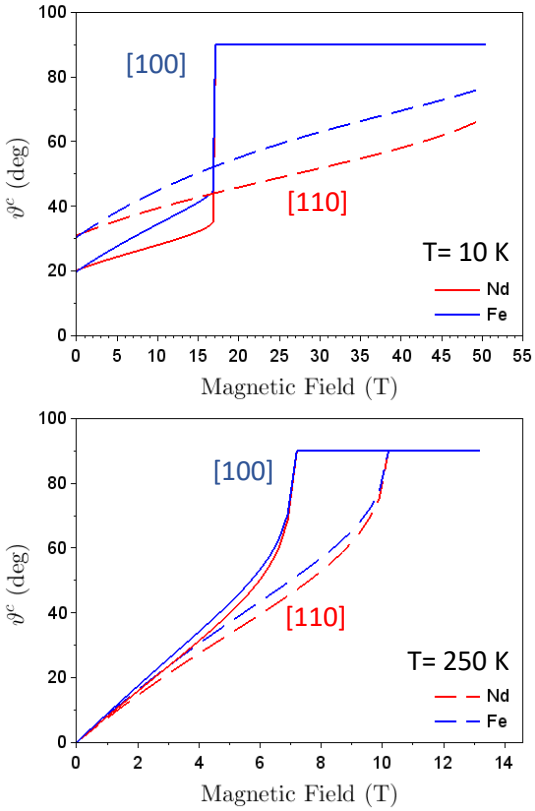

Figure 4. Evolution of the critical angle of Fe and Nd moments as a function of the magnetic field at 10 and 250 K, along the [100] (solid lines) and [110] (dashed lines) directions.

5. Ce and Co dopping

In this section we present additional results concerning the anisotropy constants of the three dopped single crystals with the chemical compositions of $(Nd_{0.85}Ce_{0.15})_2Fe_{14}B$ (hereafter referred as NdCeFeB), $Nd_2(Fe_{0.9}Co_{0.1})_{14}B$ (NdFeCoB) and $(Nd_{0.85}Ce_{0.15})_2(Fe_{0.9}Co_{0.1})_{14}B$ (NdCeFeCoB), determined by EDX analysis. In order to analyze samples with Ce we assume that Ce atoms make no contribution to the total anisotropy, nor to the total magnetization. This idea is supported by the temperature evolution of the anisotropy energy of $Ce_2Fe_{14}B$, which is very similar to that of $Lu_2Fe_{14}B$, which contains non-magnetic Lu [33,34]. We set all the anisotropy

constants of Ce to zero, and as in the case of $Nd_2Fe_{14}B$, we consider that the contribution of the 3*d* sub-lattice is the same as the anisotropy energy of $Y_2Fe_{14}B$. Due to the delocalized character of the 4*f* electron of Ce, the saturation magnetization of $Ce_2Fe_{14}B$ is slightly lower than that of the latter. Thus, we make a correction to the 3*d* sublattice magnetization:

$$M_{3d} = M_{Fe}(1 - x_{Ce}) + x_{Ce}M_{Ce}$$

where M_{Fe}=30.8μ_B and M_{Ce}=30μ_B stand for the saturation magnetization of $Y_2Fe_{14}B$ and $Ce_2Fe_{14}B$ compounds, respectively. The reported value of the magnetic moment of Ce is extremely low ($\mu_{Ce} \approx 0.1\mu_B$) [35]. Accordingly, the R magnetization is reduced by an amount proportional to the Ce content:

$$M_R = M_{Nd}(1 - x_{Ce}) \quad (8)$$

where the magnetization of Ce is taken to be zero. After these corrections, we calculate M(H) curves at different temperatures in order to obtain the corresponding anisotropy constants of Ce dopped single crystals. For the calculation we neglect the rather small changes in volume due to Ce and Co doping, which are of the order of 0.5% [10,36]. In Fig. 5 and 6 we show the uniaxial anisotropy constants K_1 to K_3 and the in-plane constants K_2' and K_3', respectively.

Since the values of K_1 are affected by those of K_2 and K_3 at finite temperature, as demonstrated by Miura et al. [37], we present in Fig. 7 the temperature evolution of the uniaxial contribution to the total anisotropy energy (K_1+K_2+K_3) separated from the in-plane contribution (K_2'+K_3'). As a general trend, the in-plane component of the anisotropy energy quickly decreases with increasing temperature. Above T_{SR} the uniaxial component dominates the total anisotropy energy whereas the in-plane component almost vanishes.

For the NdCeFeB single crystal, we see that the overall behaviour of the uniaxial anisotropy contribution closely follows that of the NdFeB parent single crystal for almost the whole temperture range, except for temperatures below 50 K. The uniaxial character of the compound is preserved. The in-plane anisotropy is significantly reduced by Ce substitution. At RT the largest reduction of the uniaxial energy is detected for this single crystal (see inset in Fig. 7).

The results for the NdFeCoB single crystal show that doping with Co significantly decreases the absolute value of all the anisotropy constants at low temperatures, and so the total uniaxial anisotropy. However, a small increase of the uniaxial energy at RT is observed (see inset of Fig 7). This result is consistent with the literature, as some beneficial effect of Co substitution is observed up to $\approx 15\%$, atributted to the preferential substitution of Co on the six non-equivalent M-sites [38]. It is important to remark that this increased anisotropy is due to the 3*d* lattice, rather than the R element. However, in our calculations, this increase of 3*d* anisotropy is not included in the model so that it is reflected in the value of the anisotropy constants of Nd. Concerning the in-plane anisotropy, it is reduced as much as for the Ce doped compound.

The double substituted NdCeFeCoB single crystal shows a very interesting behaviour. At low temperature the presence of Ce and Co results in an increase of the absolute value of the

uniaxial energy. At RT the lost anisotropy due to Ce dopping is partially recovered by the addition of Co. This is an important result for applications, as permament magnets with acceptable properties can be produced at a lower cost. Surprisingly, the in-plane contribution to the anisotropy energy closely follows that of the undoped sample.

As mentioned above, in Co substituted samples, Co shows a preference to occupy 4*c*, 8j_1 and 16k_2 sites [10,11]. The 4*c* and 8j_1 sites are the most influenced by R atoms, as they are surrounded by 4 and 3 of them, respectively. In addition, it has been shown in the literature that, Ce dopant tends to occupy 4*g* sites in the $Nd_2Fe_{14}B$ crystal structure [39], the volume of which is smaller than that of the 4*f* sites, preferred by Nd. The contribution to the total anisotropy coming from the 4*f* sites has been reported to be much larger than that of 4*g* sites [40]. The combined effect of the two substitutions described above explains the preservation of the anisotropy of the $Nd_2Fe_{14}B$ compound when a small amount of Ce and Co is introduced. It appears also that the proximity between Ce and Co at low concentrations is beneficial for the anisotropy of the compound, as signaled by Alam et al [12]. Our results show that the modification of the individual anisotropy constants due to Ce and Co co-dopping is rather complicated. As a general remark, we observe that this double substitution produces a material with good potential for applications above RT.

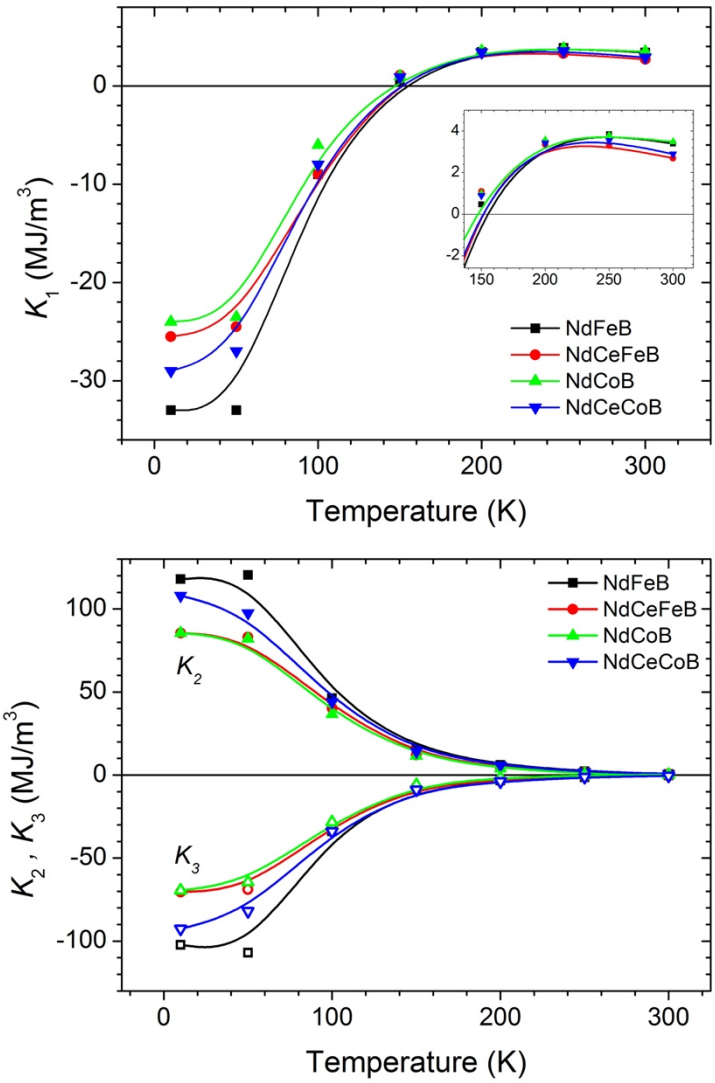

Figure 5. Evolution of the uniaxial anisotropy constants, K_1 (top), K_2 and K_3 (bottom), as a function of temperature. Results are presented for four different single crystals $Nd_2Fe_{14}B$ (black), $(Nd_{0.85}Ce_{0.15})_2Fe_{14}B$ (red), $Nd(Fe_{0.9}Co_{0.1})_{14}B$ (green) and $(Nd_{0.85}Ce_{0.15})_2(Fe_{0.9}Co_{0.1})_{14}B$ (blue). Lines are a guide to the eye.

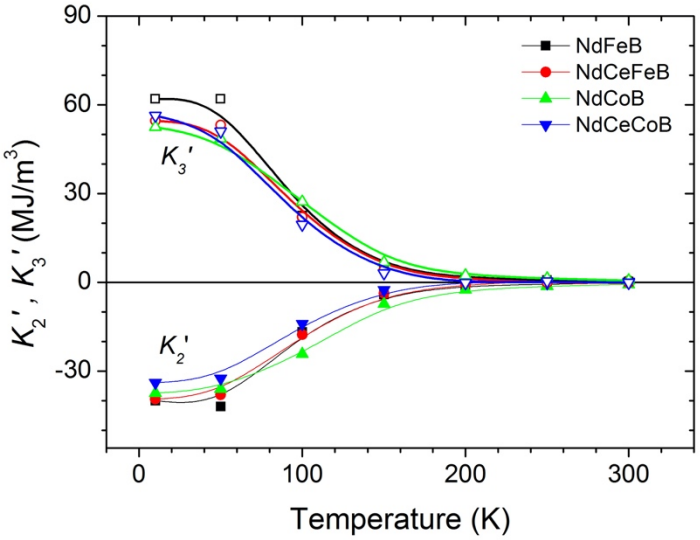

Figure 6. Evolution of the in-plane anisotropy constants, K_2' and K_3', as a function of temperature. Results are presented for four different single crystals $Nd_2Fe_{14}B$ (black), $(Nd_{0.85}Ce_{0.15})_2Fe_{14}B$ (red), $Nd(Fe_{0.9}Co_{0.1})_{14}B$ (green) and $(Nd_{0.85}Ce_{0.15})_2(Fe_{0.9}Co_{0.1})_{14}B$ (blue). Lines are a guide to the eye.

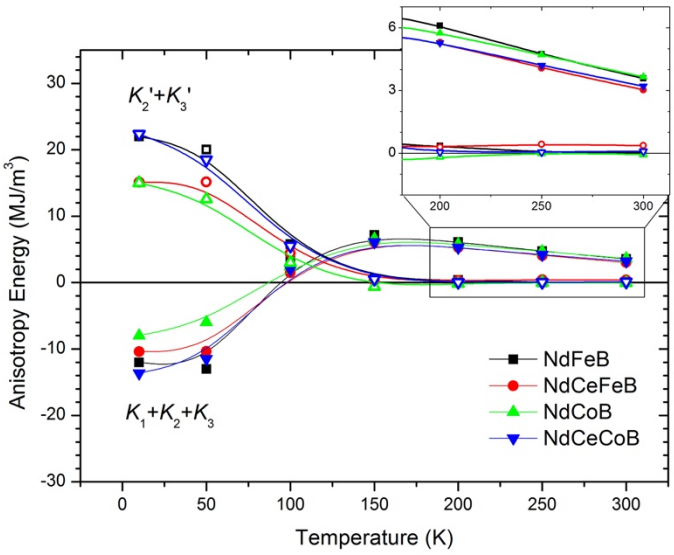

Figure 7. Evolution of uniaxial and in-plane anisotropy energies as a function of the temperature. Results are presented for four different single crystals $Nd_2Fe_{14}B$ (black), $(Nd_{0.85}Ce_{0.15})_2Fe_{14}B$ (red), $Nd(Fe_{0.9}Co_{0.1})_{14}B$ (green) and $(Nd_{0.85}Ce_{0.15})_2(Fe_{0.9}Co_{0.1})_{14}B$ (blue). Lines are a guide to the eye.

Conclusions

By applying a two sublattice model to fit experimental M(H) curves measured on single crystals, we extracted anisotropy constant values specific to the R sublattice. The anisotropy of the R sublattice is much stronger than previously reported based on single lattice extraction, and is in qualitative agreement with first principle calculations. A detailed analysis of the effect of Co and/or Ce substitution in the parent $Nd_2Fe_{14}B$ compound was presented. Surprisingly, a small amount of Ce does not signifcantly change the uniaxial anisotropy constants. At room temperature, Ce reduces the uniaxial anisotropy of the material. Co substitution deteriorates the anisotropy and magnetization of the material below 200 K, but, remarkably, at room temperature, the substitution of a small amount of Co is benefitial for the anisotropy and total magnetization. Following the general trend, this benefitial effect is expected to persist to higher temperatures. In the studied range of temperatures, the inclusion of Co in the Ce susbtituted sample helps to partially recover the lost uniaxial anisotropy. This result shows that the enhancement in the performance of NdFeB based magnets resulting from the simultaneous subsistution of Ce and Co, is due to an inprovement in the material's intrinsic properties. Our approach of extracting anisotropy constants from single crystal measurements may be used to guide the development of permanent magnets which are less dependent on critical materials.

Acknowledgements

This work was initiated together with Dominique Givord, we are grateful for his inspiration, support and friendship. This study is based on results obtained from the future pioneering program "Development of magnetic material technology for high-efficiency motors" (MagHEM), grant number JPNP14015, commissioned by the New Energy and Industrial Technology Development Organization (NEDO), Japan. This project was also supported by the Deutsche Forschungsgemeinschaft (DFG, German Research Foundation)-Project-ID 405553726-TRR 270, Germany. We acknowledge the support of the HLD at HZDR, Germany, a member of the European Magnetic Field Laboratory (EMFL).

References

1. O. Gutfleisch, M. A. Willard, E. Brück, et al., *Magnetic Materials and Devices for the 21st Century: Stronger, Lighter, and More Energy Efficient.* Advanced Materials, **23**(7), 821(2011).

2. J.M.D. Coey, *Permanent magnets: Plugging the gap.* Scripta Materialia, **67**(6), 524 (2012).

3. K. Binnemans, *Economics of rare earths: The balance problem*. in The 1st European rare earth resources conference. p. 37, Milos, Greece (2014).

4. T. W. Capehart, R. K. Mishra, G. P. Meisner, et al., *Steric variation of the cerium valence in $Ce_2Fe_{14}B$ and related compounds.* App. Phys. Lett. **63**, 3642 (1993).

5. X. Fan, S. Guo, K. Chen, R. Chen, D. Lee, C. You, and A. Yan, *Tuning Ce distribution for high performanced Nd-Ce-Fe-B sintered magnets.* Journal of Magnetism and Magnetic Materials, **419**, 394(2016).

6. M. N. Yang, H. Wang, Y. F. Hu, L. Y. M. Yang, A. Maclennan, and B. Yang, *Increased coercivity for Nd-Fe-B melt spun ribbons with 20 at.% Ce addition: The role of compositional fluctuation and Ce valence state.* Journal of Alloys and Compounds **710**, 519 (2017).

7. Y. Zhang, T. Ma, J. Jin, J. Li, C. Wu, B. Shen, and M. Yan, *Effects of $REFe_2$ on microstructure and magnetic properties of Nd-Ce-Fe-B sintered magnets.* Acta Materialia, **128**, 22(2017).

8. X. Tang, H. Sepehri-Amin, M. Matsumoto, T. Ohkubo, and K. Hono, *Role of Co on the magnetic properties of Ce-substituted Nd-Fe-B hot-deformed magnets.* Acta Materialia **175**, 1 (2019).

9. A. K. Pathak, K. A. Gschneidner, Jr., M. Khan, R. W. McCallum, and V. K. Pecharsky, *High performance Nd-Fe-B permanent magnets without critical elements.* Journal of Alloys and Compounds, **668**, 80 (2016).

10. J. F. Herbst, and W. Yelon. *Preferential site occupation and magnetic structure of $Nd_2(Co_x Fe_{1-x})_{14}B$ systems*. J. App. Phys. **60**, 4224 (1986).

11. G. G. Eslava, M. Ito, C. V. Colin, et al., *Preferential Co and Fe atom occupancy in $R_2(Fe_{1-x}Co_x)_{14}B$ intermetallic compounds (R = Nd, Y and Ce).* Accepted to Journal of Alloys and Compounds (2020).

12. A. Alam, and D. D. Johnson, *Mixed valency and site-preference chemistry for cerium and its compounds: A predictive density-functional theory study.* Phys. Rev. B **89**, 235126 (2014)

13. K. P. Skokov, and O. Gutfleisch, *Heavy rare earth free, free rare earth and rare earth free magnets - Vision and reality.* Scripta Materialia 154, 289 (2018)

14. A.K. Pathak, M. Khan, K. A. Gschneidner Jr., et al., *Cerium: An Unlikely Replacement of Dysprosium in High Performance Nd-Fe-B Permanent Magnets.* Advanced Materials **27**(16), 2663 (2015).

15. A. K. Pathak, M. Khan, K. A. Gschneidner Jr., et al., *Magnetic properties of bulk, and rapidly solidified nanostructured $(Nd_{1-x} Ce_x)_2Fe_{14-y}Co_yB$ ribbons.* Acta Materialia, **103**, 211 (2016).

16. M. Ito, M. Yano, N. M. Dempsey, and D. Givord, *Calculations of the magnetic properties of $R_2M_{14}B$ intermetallic compounds (R1⁄4rare earth, M1⁄4Fe, Co),* J.Mag. Mag. Mat. **400**, 379 (2016).

17. G. Gomez Eslava, M. Ito, M. Yano, N. M. Dempsey, and D. Givord, *Calculation of the magnetic properties of pseudo-ternary R2M14B intermetallic compounds (R = rare earth, M= Fe, Co)*, Journal of Science: Advanced Materials and Devices **1**,158 (2016).

18. M. G. Kanatzidis, R. Pöttgen, and W. Jeitschko, *The Metal Flux: A Preparative Tool for the Exploration of Intermetallic Compounds.* Angewandte Chemie International Edition **44**(43), 6996 (2005)

19. Y. Skourski, M. D. Kuz'min, K. P. Skokov, A. V. Andreev, and J. Wosnitza, *High-field magnetization of Ho_2Fe_{17}.* Physical Review B, **83**(21), 214420 (2011)

20. F. Bolzoni, O. Moze, and L. Pareti. *First-order field-induced magnetization transitions in singlecrystal $Nd_2Fe_{14}B$*, J. App. Phys. **62**, 615 (1987).

21. J. M. Cadogan, J. P. Gavigan, D. Givord, H. S. Li, *A new approach to the analysis of magnetisation measurements in rare-earth/transition-metal compounds: application to $Nd_2Fe_{14}B$*, J.Phys.F: Met. Phys. **18**, 779 (1988).

22. M. Yamada, H. Kato, H. Yamamoto, and Y. Nakagawa, *Crystal-field analysis of the magnetization process in a series of $Nd_2Fe_{14}B$-type compounds*. Phys. Rev. B **38**, 620 (1988).

23. J. F. Herbst, *$R_2Fe_{14}B$ materials: Intrinsic properties and technological aspects.* Rev. Mod. Phys.

63, 819 (1991).

24. D. Miura, and A. Sakuma, *Non-collinearity Effects on Magnetocrystalline Anisotropy for $R_2Fe_{14}B$ Magnets*. Journal of the Physical Society of Japan 88, 044804 (2019).

25. S. Hirosawa, Y. Matsuura, H. Yamamoto, S. Fujimura, M. Sagawa, and H. Yamauchi. *Magnetization and magnetic anisotropy of $R_2Fe_{14}B$ measured on single crystals.* J. Appl. Phys. **59**, 873 (1986).

26. M. D. Kuz'min, *Shape of Temperature Dependence of Spontaneous Magnetization of Ferromagnets: Quantitative Analysis*. Phys. Rev. Lett. **94**, 107204 (2005).

27. M. D. Kuz'min, D. Givord, and V. Skumryev. *Why the iron magnetization in Gd 2 Fe 14 B and the spontaneous magnetization of Y_2Fe_{14} B depend on temperature differently.* J. App. Phys. **107**, 113924 (2010).

28. E. Belorizky, M. A. Fremy, J. P. Gavigan, D. Givord, and H. S. Li, *Evidence in rare earth (R)–transition metal (M) intermetallic s for a systematic dependence of RM exchange interactions on the nature of the R atom.* Journal of App. Phys. **61**, 3971 (1987).

29. C. H. de Groot and K. de Kort, *Magnetoelastic anisotropy in NdFeB permanent magnets*. J. Appl. Phys., **85**, 8312 (1999).

30. Yuta Toga, Munehisa Matsumoto, Seiji Miyashita, et al., *Monte Carlo analysis for finite-temperature magnetism of $Nd_2Fe_{14}B$ permanent magnet.* Phys. Rev. B **94**, 174433 (2016)

31. Q. Gong, M. Yi, R. F. L. Evans, et al., *Calculating temperature-dependent properties of $Nd_2Fe_{14}B$ permanent magnets by atomistic spin model simulations*, Phys. Rev. B **99**, 214409 (2019)

32. K. D. Durst, and H. Kronmuller, *Determination of intrinsic magnetic material parameters of $Nd_2Fe_{14}B$ from magnetic measurements of sintered $Nd_{15}Fe_{77}B_8$ magnets*. J. Magn. Magn. Mater **59**, 86(1986)

33. R. Grössinger, X. Sun, R. Eibler, K. Buschow, and H. Kirchmayr, *The temperature dependence of the anisotropy field in $R_2Fe_{14}B$ compounds (R = Y, La, Ce, Pr, Nd, Gd, Ho, Lu)*, Journal de Physique Colloques, **46**, C621 (1985).

34. L. Pareti, O. Moze, M. Solzi, F. Bolzoni, G. Asti, and G. Marusi, *Macroscopic Studies of Magnetic Anisotropy in Rare-Earth Intermetallic Compounds*. In: I.V. Mitchell, J.M.D. Coey, D. Givord, I. R. Harris, R. Hanitsch (eds.), Concerted European Action on Magnets (CEAM), p.p. 188, Springer, Dordrecht (1989).

35. J. Wang, L. Liang, L.T. Zhang, M. Yano, K. Terashima, H. Kada, S. Kato, T. Kadono, S. Imada, T. Nakamura, and S. Hirano, *Mixed-valence state of Ce and its individual atomic moments in Ce2Fe14B studied by soft X-ray magnetic circular dichroism.* Intermetallics **69**, 42 (2016).

36. M. A. Susner, B. S.Connera, B.I. Saparov et al., *Flux growth and characterization of Ce-substituted single crystals*. J. of Magn. and Magn. Mat. 434, 1 (2017).

37. D. Miura, R. Sasaki, and A. Sakuma, *Direct expressions for magnetic anisotropy constants.* App. Phys. Exp. 8, 113003 (2015).

38. M. H. Hong, J. J. M. Franse, and P. T. Nguyen. *Magnetic anisotropy of the $Y_2(Co_{1-x}Fe_x)_{14}B$ intermetallic compounds*, J .Less-Comm. Met. 155,151 (1989).

39. C. V. Colin, M. Ito, M. Yano, N. M. Dempsey, E. Suard, and D. Givord, *Solid-solution stability and preferential site-occupancy in (R-R')$_2$Fe$_{14}$B compounds.* Appl. Phys. Lett. **108**, 242415 (2016).

40. D.Haskel, J. C. Lang, Z. Islam, et al. *Atomic Origin of Magnetocrystalline Anisotropy in Nd$_2$Fe$_{14}$B*, Phys. Rev. Lett. **95,** 217207 (2005).